



CHORUS

This is the accepted manuscript made available via CHORUS. The article has been published as:

Fast-timing measurements in the ground-state band of ^{114}Pd

E. R. Gamba *et al.*

Phys. Rev. C **100**, 044309 — Published 11 October 2019

DOI: [10.1103/PhysRevC.100.044309](https://doi.org/10.1103/PhysRevC.100.044309)

Fast-timing measurements in the ground-state band of ^{114}Pd

E. R. Gamba,¹ A. M. Bruce,^{1,*} S. Lalkovski,^{2,†} M. Rudigier,² S. Bottoni,^{3,‡} M. P. Carpenter,³
S. Zhu,³ J. T. Anderson,³ A. D. Ayangeakaa,^{3,§} T. A. Berry,² I. Burrows,⁴ M. Carmona Gallardo,⁵
R. J. Carroll,² P. Copp,⁶ D. M. Cullen,⁷ T. Daniel,^{2,¶} G. Fernández Martínez,⁸ J. P. Greene,³ L. A. Gurgi,²
D. J. Hartley,⁹ R. Ilieva,² S. Ilieva,⁸ F. G. Kondev,¹⁰ T. Kröll,⁸ G. J. Lane,¹¹ T. Lauritsen,³ I. Lazarus,⁴
G. Lotay,² C. R. Niță,¹² Zs. Podolyák,² V. Pucknell,⁴ M. Reed,¹¹ P. H. Regan,^{2,13} J. Rohrer,³ J. Sethi,³
D. Seweryniak,³ C. M. Shand,² J. Simpson,⁴ M. Smoleń,¹⁴ E. A. Stefanova,¹⁵ V. Vedia,⁵ and O. Yordanov¹⁵

¹*School of Computing, Engineering and Mathematics,
University of Brighton, Brighton BN2 4GJ, United Kingdom*

²*Department of Physics, University of Surrey, Guildford GU2 7XH, United Kingdom*

³*Physics Division, Argonne National Laboratory, Argonne, Illinois 60439, USA*

⁴*STFC Daresbury Laboratory, Daresbury, Warrington WA4 4AD, United Kingdom*

⁵*Grupo de Física Nuclear, Universidad Complutense, CEI Moncloa, ES-28040 Madrid, Spain*

⁶*Department of Physics and Applied Physics, University of Massachusetts Lowell, Lowell, Massachusetts 01854, USA*

⁷*School of Physics and Astronomy, University of Manchester, Manchester M13 9PL, United Kingdom*

⁸*Institut für Kernphysik, TU Darmstadt, Schlossgartenstrasse 9, 64289 Darmstadt, Germany*

⁹*Department of Physics, U.S. Naval Academy, Annapolis, Maryland 21402, USA*

¹⁰*Nuclear Engineering Division, Argonne National Laboratory, Argonne, Illinois 60439, USA*

¹¹*Department of Nuclear Physics, R.S.P.E., Australian National University, Canberra 0200, Australia*

¹²*Horia Hulubei National Institute of Physics and Nuclear Engineering, Bucharest-Măgurele, Romania*

¹³*AIR Division, NPL, Teddington, TW11 0LW, United Kingdom*

¹⁴*School of Engineering and Science, University of the West of Scotland, Paisley PA1 2BE, United Kingdom*

¹⁵*INRNE, Bulgarian Academy of Sciences, 1784 Sofia, Bulgaria*

(Dated: September 1, 2019)

Using a hybrid Gammasphere array coupled to 25 LaBr₃(Ce) detectors, the lifetimes of the first three levels of the yrast band in ^{114}Pd , populated via ^{252}Cf decay, have been measured. The measured lifetimes are $\tau_{2+} = 103(10)$ ps, $\tau_{4+} = 22(13)$ ps and $\tau_{6+} \leq 10$ ps for the 2_1^+ , 4_1^+ and 6_1^+ levels, respectively. Palladium-114 was predicted to be the most deformed isotope of its isotopic chain and spectroscopic studies have suggested it might also be a candidate nucleus for low-spin stable triaxiality. From the lifetimes measured in this work, reduced transition probabilities $B(E2; J \rightarrow J-2)$ are calculated and compared with IBM, PSM and Collective model calculations from the literature. The experimental ratio $R_{B(E2)} = B(E2; 4_1^+ \rightarrow 2_1^+)/B(E2; 2_1^+ \rightarrow 0_1^+) = 0.80(42)$ is measured for the first time in ^{114}Pd and compared with the known values $R_{B(E2)}$ in the palladium isotopic chain: the systematics suggest that, for $N = 68$, a transition from γ -unstable to a more rigid γ -deformed nuclear shape occurs.

I. INTRODUCTION

Nuclear lifetimes are very important physical observables able to provide fundamental information on the structure of the atomic nucleus. The lifetime of a nuclear excited level can be related to the quadrupole reduced transition probability $B(E2; J \rightarrow J-2)$ of the level, which is in turn related to the intrinsic quadrupole moment Q_0 . This is strictly dependent on the quadrupole deformation parameter β_2 [1]. By measuring the lifetime

of nuclear excited levels it is therefore possible to quantify the occurrence of deformation across the nuclear chart as a function of proton and neutron numbers. Nuclear deformation has been studied systematically in regions far from shell closures such as $A \simeq 110$, $A \simeq 150$ and $A \simeq 250$, where nuclei are known to be characterized by non-spherical shapes [2]. Together with oblate ($\beta_2 < 0$) and prolate ($\beta_2 > 0$) deformed nuclei, a third possibility is represented by cases of static or dynamical triaxial deformation ($\gamma \neq n\frac{\pi}{3}$), where all three nuclear axes have different lengths. Indications of triaxial deformation have been observed in the molybdenum ($Z = 42$) [3, 4], ruthenium ($Z = 44$) [5–7] and palladium ($Z = 46$) [8] isotopic chains.

The palladium isotopic chain lies between Cd ($Z = 48$), usually treated as vibrational [9], and Ru ($Z = 44$) showing γ -soft and rigid-triaxial rotor behaviour [5, 6]. Studies have indicated the vibrational behaviour of $^{106,108}\text{Pd}$ isotopes [10] which approaches that of a γ -soft rotor for $A \leq 110$ [8]. Spectroscopic investigations of higher mass $^{116-120}\text{Pd}$ isotopes [11–13] suggest that, as the neutron

* Alison.Bruce@brighton.ac.uk

† Present address: Department of Nuclear Engineering, Faculty of Physics, University of Sofia “St. Kl. Ohridski”, Sofia 1164, Bulgaria

‡ Present address: Dipartimento di Fisica, Università degli Studi di Milano and INFN, 20133, Milano, Italy

§ Present address: Department of Physics, U.S. Naval Academy, Annapolis, Maryland 21402, USA

¶ Present address: Department of Physics, Benue State University, P.M.B, 102119, Makurdi, Nigeria.

number increases, the behaviour of Pd isotopes moves back to that of an anharmonic vibrator showing a loss of collectivity [14].

The isotope ^{114}Pd ($N = 68$) lies very close to the mid shell at $N = 66$, between the $N = 50$ and $N = 82$ neutron shell closures, and it has been shown in Ref. [15] that the maximum of rotational collectivity is reached for this isotope. Furthermore, for $N = 68$, the maximum value of the ratio $E(4_1^+)/E(2_1^+) \simeq 2.6$ is reached [15]. Similarly to the case of the ruthenium isotopic chain, this never reaches the rotational limit of 3.33, which is expected for axially symmetric nuclei.

From a spectroscopic perspective, for the isotope ^{114}Pd , the energy spacing of the yrast band follows quite remarkably the $\sim J(J+6)$ pattern expected for both Willets-Jean's γ -soft [16] and Davydov-Filippov's rigid triaxial rotor [17] models. Two important signatures for triaxial deformation are also the $E_{2_2^+}/E_{4_1^+}$ and $E_{2_2^+}/E_{2_1^+}$ ratios which, for this case, are 0.8 and 2.1, respectively. The former is reported by both Willets-Jean's and Davydov-Filippov's models to be a signature of strong departure from axially, while the latter is consistent with a γ deformation parameter of 27.5° .

A distinction between γ -soft and rigid triaxial behaviour can be established when looking at the energy spacing between levels inside the quasi- γ band [18]. In Ref. [19] Pd isotopes have been systematically analysed in terms of the *staggering parameter* $S(J)$, defined as

$$S(J) = \frac{(E(J) - 2E(J-1) + E(J-2))}{E(2_1^+)}, \quad (1)$$

where $E(J)$ is the energy of a level with spin J in the quasi- γ band. In the case of γ -soft nuclei, the $S(J)$ parameter is expected to take positive values for the odd-spin levels and negative values for the even-spin ones, while the opposite is true for the γ -rigid case [20]. Figure 1 shows the behaviour of the parameter $S(J)$ for the quasi- γ band in the nuclei $^{108-118}\text{Pd}$. An inversion of the type of triaxiality, from γ -soft to that of a rigid rotor, is observed for ^{114}Pd .

In this work, ^{114}Pd nuclei were produced via the spontaneous fission of ^{252}Cf , which is able to populate the regions of deformed nuclei around mass numbers $A \simeq 110$ and $A \simeq 150$ with higher fission yields for neutron-rich nuclei with respect to other neutron-induced fission reactions [21]. The measured lifetimes of the 2_1^+ , 4_1^+ and 6_1^+ levels, are used to calculate $B(E2; J \rightarrow J-2)$ transition probabilities and then compared with theoretical calculations from the literature, performed using the Interacting Boson Model (standard and triaxial IBM-1) [22, 23], the Projected Shell Model (PSM) [24] and the Collective model [2, 25] with the inclusion of the Killingbeck potential [26]. Since $R_{B(E2)} = B(E2; 4_1^+ \rightarrow 2_1^+)/B(E2; 2_1^+ \rightarrow 0_1^+)$ ratios are known to be able to give information about the type of nuclear deformation, and are well established for nuclei in the mass region $A \simeq 110$, of prime interest for the present work is to obtain new

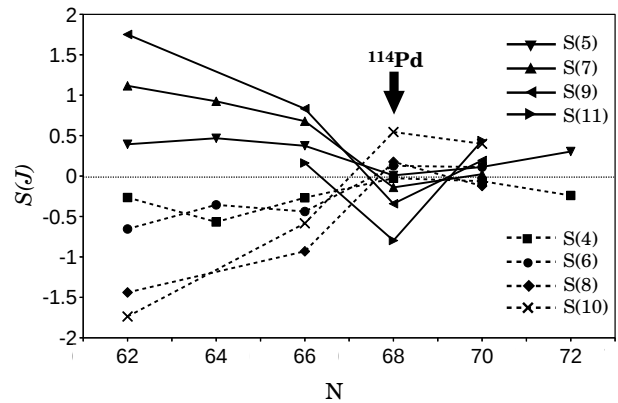


FIG. 1. Values of $S(J)$ for $^{108-118}\text{Pd}$ nuclei, calculated from Eq. 1, using values taken from Ref. [27]. The staggering parameter for odd- J levels (solid lines) are compared with those for even- J levels (dashed lines). Figure adapted from Ref. [19].

information on the $R_{B(E2)}$ ratio for ^{114}Pd . Furthermore, the experimental $R_{B(E2)}$ ratio obtained for ^{114}Pd is compared with those from the neighbouring even- N palladium isotopes, when these are available, and with the theoretical values predicted by the vibrational, rigid axial rotor, Davydov-Filippov's and Willets-Jean's models.

II. EXPERIMENTAL SET-UP

The experimental set-up combined the Gammasphere [28] and FATIMA [29, 30] arrays at the Argonne National Laboratory (USA). This was the first time that Gammasphere was coupled to such a large number of $\text{LaBr}_3(\text{Ce})$ scintillator detectors using a fully-digital acquisition set-up. ^{114}Pd nuclei were observed following the spontaneous fission of a $34.4 \mu\text{Ci}$ ^{252}Cf source placed at the centre of a 4π hybrid array made of 51 Compton-suppressed HPGe detectors from the Gammasphere array coupled to 25 $\text{LaBr}_3(\text{Ce})$ scintillator detectors from the FATIMA array.

The source consisted of a sample of 183 ng of ^{252}Cf electrodeposited on a platinum disk of ~ 1.6 cm diameter and 0.25 mm thickness with an active spot of ~ 1.27 cm diameter. A second platinum disk of the same size was attached to the other side of the source using an indium layer of $250 \mu\text{m}/\text{cm}^2$. The resulting disk sandwiched the source between the two Pt disks, therefore fission fragments were equally absorbed on both sides of the disk and no Doppler-shifted γ -rays nor increased line widths were observed.

Each $\text{LaBr}_3(\text{Ce})$ detector consisted of a cylindrical crystal 3.8 cm in diameter and 5.1 cm in length, coupled with a Hamamatsu H10570 photomultiplier assembly comprising a R9779 phototube. A 5 mm-thick lead layer covered the side of each $\text{LaBr}_3(\text{Ce})$ crystal in order to absorb Compton-scattered γ -rays from ad-

155 jacent crystals. A fully digital acquisition system (DAQ)
 156 was used on the entire $\text{LaBr}_3(\text{Ce})$ array for the first
 157 time. On the $\text{LaBr}_3(\text{Ce})$ side, events made of at least
 158 two γ rays within a time window of 200 ns were col-
 159 lected. Independently, fold ≥ 1 events were collected in
 160 the Gammasphere array. The two DAQ data streams
 161 were eventually merged using a coincidence time win-
 162 dow of 500 ns between the fold ≥ 2 - $\text{LaBr}_3(\text{Ce})$ and
 163 fold ≥ 1 -HPGe events, in order to give events of the type
 164 $\gamma(\text{LaBr}_3(\text{Ce}))$ - $\gamma(\text{LaBr}_3(\text{Ce}))$ - $\gamma(\text{HPGe})$. During a 30-day
 165 long run a total of 2.6×10^9 $E_\gamma(\text{HPGe})$ - $E_\gamma(\text{LaBr}_3(\text{Ce}))$ -
 166 $E_\gamma(\text{LaBr}_3(\text{Ce}))$ events were collected. For a detailed de-
 167 scription of the acquisition system see Ref. [31].

168 III. DATA ANALYSIS AND RESULTS

169 The level of statistics obtained in this experiment only
 170 allowed the lifetimes of the 2_1^+ , 4_1^+ and 6_1^+ levels in ^{114}Pd
 171 to be measured. In order to measure the three life-
 172 times, both $\text{LaBr}_3(\text{Ce})$ and HPGe detectors were used.
 173 Due to the superior energy resolution of HPGe detectors,
 174 $E_\gamma(\text{HPGe})$ transitions were used to select the nucleus
 175 of interest and the corresponding excited band, while
 176 cerium-doped lanthanum bromide ($\text{LaBr}_3(\text{Ce})$) scintil-
 177 lator detectors, capable to access the sub-nanosecond
 178 range, were used to measure the lifetimes of interest.
 179 The large number of contaminant γ -ray peaks from the
 180 large number of fission fragments means that particu-
 181 lar care had to be taken when applying the $E_\gamma(\text{HPGe})$
 182 gates and when performing the lifetime measurements
 183 with the $\text{LaBr}_3(\text{Ce})$ detectors. The lifetimes measured
 184 in this work were around 100 ps or shorter, therefore
 185 the *Generalized Centroid Difference* (GCD) method [32]
 186 was used. The background correction applied on the
 187 time information followed the *Three Samples* approach
 188 described in Ref. [33].
 189 The analysis performed for the three levels used simi-
 190 lar procedures, however, for each case, individual adjust-
 191 ments had to be considered. For the discussions carried
 192 out in this Section, the reader should refer to the partial
 193 level scheme of ^{114}Pd , presented in Fig. 2, where only
 194 the levels and transitions of interest for this work are
 195 represented.

196 A. 2_1^+ level in ^{114}Pd

197 For the lifetime measurement of the 2_1^+ level in ^{114}Pd ,
 198 $E_\gamma(\text{HPGe})$ gates were applied on the $6_1^+ \rightarrow 4_1^+$ (648 keV),
 199 $8_1^+ \rightarrow 6_1^+$ (715 keV), $10_1^+ \rightarrow 8_1^+$ (644 keV) and $5_1^- \rightarrow 4_1^+$
 200 (1332 keV) transitions. For each of these Full-Energy
 201 Peak (FEP) gates a $E_\gamma(\text{HPGe})$ background gate was also
 202 identified. Each of these background gates was taken as
 203 close as possible to the corresponding FEP gate and the
 204 same gate width (usually 2 or 3 keV) was used. Due
 205 to the large number of peaks in the ^{252}Cf fission spec-
 206 trum the selection of $E_\gamma(\text{HPGe})$ background gates re-

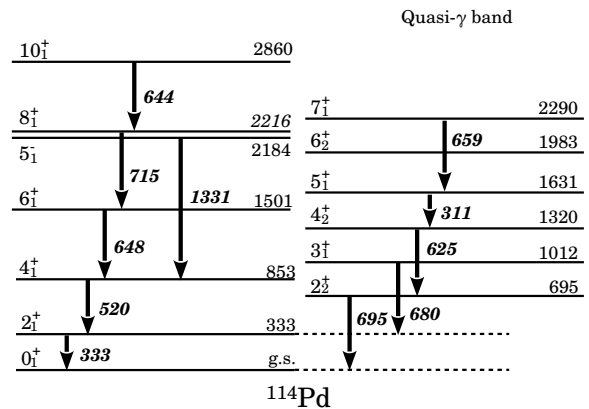


FIG. 2. Partial level scheme of ^{114}Pd , including the ground-
 state band and the quasi- γ band, of interest for this work. For
 clarity, the 5_1^- level is also included (see text for details) [27].
 All arrows have equal widths and these don't reflect the γ -ray
 intensities.

quired extreme care, to make sure that no peak with
 small amplitude was included in the background gate.
 The $E_\gamma(\text{HPGe})$ (red) and $E_\gamma(\text{LaBr}_3(\text{Ce}))$ (blue) energy
 spectra shown in Fig. 3 were obtained by adding together
 the four different FEP-gated energy spectra and by sub-
 tracting the four background-gated spectra, for both ar-
 rays, respectively. In both spectra the $4_1^+ \rightarrow 2_1^+$ (feeding
 transition at 520 keV) and $2_1^+ \rightarrow 0_{g.s.}^+$ (decay transition at
 333 keV) are clearly visible, together with other higher-
 energy transitions from the same nucleus or its fission
 partners. The same FEP and background $E_\gamma(\text{HPGe})$
 gates were then applied to produce eight $E_\gamma(\text{LaBr}_3(\text{Ce}))$ -
 $E_\gamma(\text{LaBr}_3(\text{Ce}))$ - ΔT cubes with coincident events. This
 set of eight cubes was then used to produce the final
 $E_\gamma(\text{LaBr}_3(\text{Ce}))$ - $E_\gamma(\text{LaBr}_3(\text{Ce}))$ - ΔT cube by adding to-
 gether the four cubes obtained from the FEP gates and
 subtracting those from the background gates.
 The final E_γ - E_γ - ΔT cube produced following this pro-
 cedure is a so-called start-and-stop cube, i.e. the two
 energy axes x and y represent the energy values mea-
 sured for the γ rays defining the start and stop of the
 measured ΔT value, respectively. Here, ΔT is defined as

$$\Delta T = T_{E_y} - T_{E_x}. \quad (2)$$

The information from the detector with the smaller iden-
 tification number was put on the x axis and the other
 one on the y axis. This avoids the cube from being
 filled twice and also makes it not symmetrical. The E_γ -
 E_γ matrix obtained projecting the cube on the $x - y$
 plane, for the case of the 2_1^+ level in ^{114}Pd , is shown
 in Fig. 4. The two coincidence peaks circled in red
 contain independent events from the $4_1^+ \rightarrow 2_1^+ \rightarrow 0_{g.s.}^+$
 cascade and, by gating on them, the $p|p$ (FEP-FEP) de-
 layed and anti-delayed time distributions are obtained.
 In order to background-correct the value of the centroid
 position $C_{p|p}^m$ (where the label m stands for *measured*)
 of the delayed and anti-delayed time distributions, the

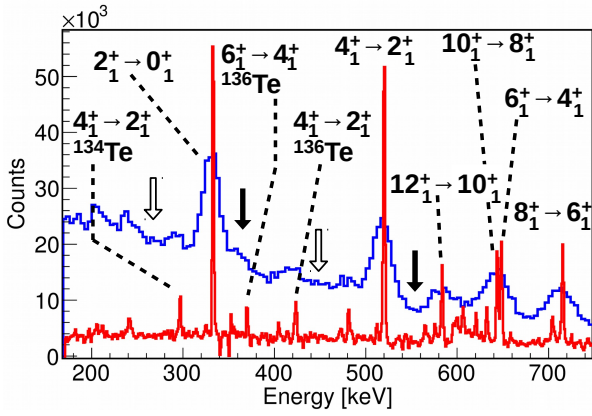


FIG. 3. (Colour online). Gammasphere (red) and LaBr₃(Ce) (blue) energy spectra, obtained by adding together four FEP(HPGe)-gated energy spectra and by subtracting four background-gated energy spectra, see text for details. The $4_1^+ \rightarrow 2_1^+$ and $2_1^+ \rightarrow 0_{g.s.}^+$ transitions in ^{114}Pd are clearly visible. It can also be noticed the large number of (small) transitions, produced by ^{114}Pd itself and the fission partners $^{134,136}\text{Te}$. For the purpose of this measurement these small peaks are considered as contaminants. The four arrows indicate the left (unfilled) and right (filled) background regions considered for the timing background subtraction (see text and Fig. 4).

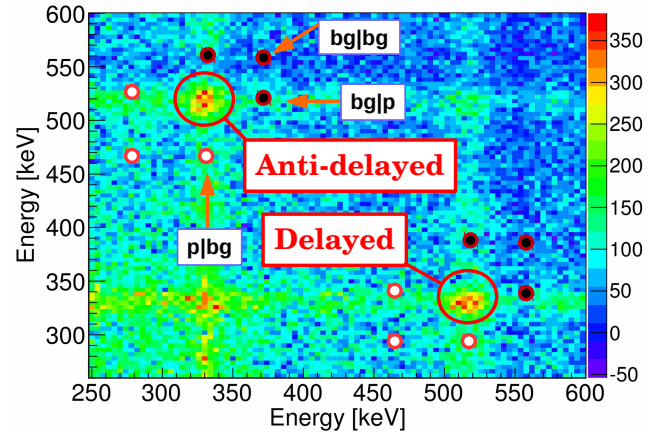


FIG. 4. (Colour online). Two-dimensional projection of the start and stop $E_\gamma(\text{LaBr}_3(\text{Ce})) - E_\gamma(\text{LaBr}_3(\text{Ce})) - \Delta T$ cube obtained by gating on the $6_1^+ \rightarrow 4_1^+$, $8_1^+ \rightarrow 6_1^+$, $10_1^+ \rightarrow 8_1^+$ and $5_1^- \rightarrow 4_1^-$ transitions, in ^{114}Pd , in Gammasphere. The two regions encircled by the red solid lines represent the coincidence peaks for the $4_1^+ \rightarrow 2_1^+ \rightarrow 0_{g.s.}^+$ cascade. The dots encircled in red are used to indicate the left (white) and right (black) gates applied to obtain the three background components, for both the delayed and anti-delayed time distributions. These correspond to the four arrows shown in Fig. 3.

272 the equation

$$C_{p|p}^t = \frac{n_{p|p}^m C_{p|p}^m - n_{p|bg}^m C_{p|bg}^m - n_{bg|p}^m C_{bg|p}^m + n_{bg|bg}^m C_{bg|bg}^m}{n_{p|p}^m - n_{p|bg}^m - n_{bg|p}^m + n_{bg|bg}^m}, \quad (3)$$

273 where $n_{p|p}^m$, represent the *measured* number of counts of
 274 the $p|p$ time distribution. In order to take into account
 275 the energy-dependent time-walk affecting the centroid
 276 position of each background time distribution, these were
 277 corrected for the Compton time-walk obtained from the
 278 Compton curve (see Ref. [33]) before being used in Eq. 3.
 279 The measured centroid positions and number of counts
 280 for each of the eight time components measured and for
 281 the final background-corrected delayed and anti-delayed
 282 time distributions, are listed in the first part of Table. I.
 283 The centroid difference value, ΔC , defined as

$$\Delta C^t = C_{p|p}^{t,del} - C_{p|p}^{t,anti-del}, \quad (4)$$

284 was then corrected for the FEP-FEP time-walk which,
 285 when the GCD method is used, is usually described by
 286 the Prompt Response Difference Curve (PRD). This cor-
 287 rection term is given by the value $\text{PRD}(E_f, E_d)$, defined
 288 as

$$\text{PRD}(E_f, E_d) = \text{PRD}(E_f) - \text{PRD}(E_d). \quad (5)$$

289 The Compton curve and the PRD curve are shown in
 290 Fig.5. Finally, the lifetime of the level is obtained from
 291 the equation

$$\tau = \frac{\Delta C^t - \text{PRD}(E_f, E_d)}{2}. \quad (6)$$

274 *Three Samples* approach explained in Ref. [33] was used.
 275 The *Interpolation* approach was avoided due to the large
 276 number of contaminant peaks. The three samples of
 277 the $p|bg$ (FEP-background), $bg|p$ (background-FEP) and
 278 $bg|bg$ (background-background) background components
 279 were obtained from the average between the left and right
 280 gates indicated by the white and black dots in Fig. 4, re-
 281 spectively. The same gates were represented in Fig. 3 by
 282 the unfilled and filled arrows.
 283 Twelve 2-dimensional background gates were considered
 284 (six for each coincidence peak) in total. For example,
 285 events showing a coincidence between the $2_1^+ \rightarrow 0_{g.s.}^+$
 286 transition and the background gate to the right (left)
 287 of the $2_1^+ \rightarrow 0_{g.s.}^+$ transition, give the right (left) gate
 288 of the $p|bg$ background component. The opposite is
 289 true for the left and right background gates of the $bg|p$
 290 component. The 2-dimensional right (left) $bg|bg$ gates
 291 shown in Fig. 4, are obtained by combining the ener-
 292 gies of two right (left) background gates shown in Fig. 3.
 293 From these six time distributions, three background time
 294 distributions were obtained from the weighted average
 295 between the two time distributions characterizing each
 296 background component. From these, the centroid posi-
 297 tions $C_{p|bg}^m$, $C_{bg|p}^m$ and $C_{bg|bg}^m$ and the number of counts
 298 $n_{p|bg}^m$, $n_{bg|p}^m$ and $n_{bg|bg}^m$ were obtained. For both delayed
 299 and anti-delayed time distributions, the *true* centroid po-
 300 sition $C_{p|p}^t$ of the time distribution was calculated from

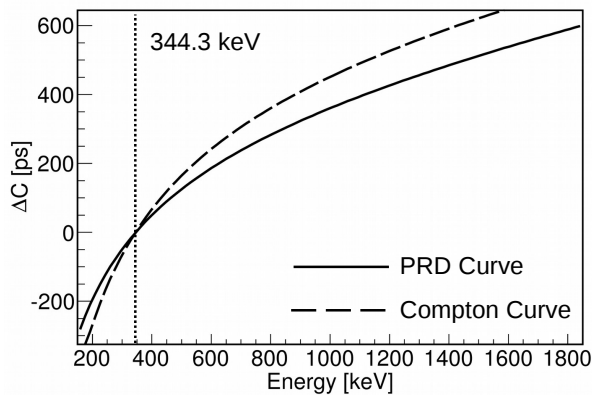


FIG. 5. Experimental PRD (solid line) and Compton (dashed line) curves, plotted using 344.3 keV as the reference energy. These are used to correct for the effect of the time-walk on the position of the centroids of the FEP ($p|p$) and background ($p|bg$, $bg|p$ and $bg|bg$) time distributions, respectively. See Refs. [32, 33] for a complete description of the properties of these two curves.

296 The corrected centroid shift value of $\Delta C^t = 358(19)$ ps,
 297 together with a time-walk correction of $\text{PRD}(520,$
 298 $333) = 152(6)$ ps, gave a lifetime for the 2_1^+ level of
 299 $\tau = 103(10)$ ps. This is consistent with the literature
 300 value of $\tau = 118(20)$ ps, from Ref. [15], and also with
 301 the result of $\tau = 116(6)$ ps obtained in Ref. [34], that
 302 was never published in a referee journal. The weighted
 303 average of the three values is $\tau_{2^+} = 113(5)$ ps and that
 304 is the value which will be used later on in the paper.

B. 4_1^+ level in ^{114}Pd

305
 306 The 4_1^+ level in ^{114}Pd was isolated by applying three
 307 background-subtracted HPGe gates on the $2_1^+ \rightarrow 0_{g.s.}^+$,
 308 $8_1^+ \rightarrow 6_1^+$ and $10_1^+ \rightarrow 8_1^+$ transitions. The resulting γ -ray
 309 spectra are shown in Fig. 6. The energy gates on the
 310 $4_1^+ \rightarrow 2_1^+$ and $6_1^+ \rightarrow 4_1^+$ transitions in $E_\gamma(\text{LaBr}_3(\text{Ce}))$ are
 311 shown by the two pairs of black solid lines. The non-
 312 negligible contribution of the 511 keV peak to the peak
 313 at 520 keV means that the energy gate on the $4_1^+ \rightarrow 2_1^+$
 314 transition was taken only to the right of the energy peak.
 315 The energy gate on the $6_1^+ \rightarrow 4_1^+$ transition was taken as
 316 narrow as possible in order to minimize the contributions
 317 from the $10_1^+ \rightarrow 8_1^+$ and $7_1^+ \rightarrow 5_1^+$ (659 keV, from the
 318 quasi- γ band) transitions. The former is presumably car-
 319 rying a very short lifetime, from the 10_1^+ level, while the
 320 lifetime carried by the latter is unknown. The position
 321 of the two background gates are indicated by the black
 322 arrows. For the $4_1^+ \rightarrow 2_1^+$ peak, this was taken as close as
 323 possible to the peak. The second background gate was
 324 applied around 750 keV of energy, in order to avoid the
 325 $3_1^+ \rightarrow 2_1^+$ transition, from the quasi- γ band at 680 keV.
 326 Only the background to the right-hand side of the coin-
 327 cidence peak was considered for the *Three Samples* ap-
 328 proach because of the large number of contaminant peaks

329 on the left-hand side of the $6_1^+ \rightarrow 4_1^+$ transition. At the
 330 same time, the asymmetric energy gate for the $6_1^+ \rightarrow 4_1^+$
 331 peak, should reduce the contribution from the left-hand-
 332 side background significantly. The position of the $p|p$,
 333 $p|bg$, $bg|p$ and $bg|bg$ gates are indicated in the projection
 334 of the $E_\gamma(\text{LaBr}_3(\text{Ce}))$ - $E_\gamma(\text{LaBr}_3(\text{Ce}))$ - ΔT cube in Fig. 7.
 335 A corrected centroid difference value of $\Delta C^t = 116(26)$
 336 ps was found for this measurement (refer to Table I).
 337 Combining this value with the time-walk correction of
 338 $\text{PRD}(648, 520) = 71(5)$ ps, Eq. 6 gives a lifetime of
 339 $\tau_{4^+} = 22(13)$ ps.

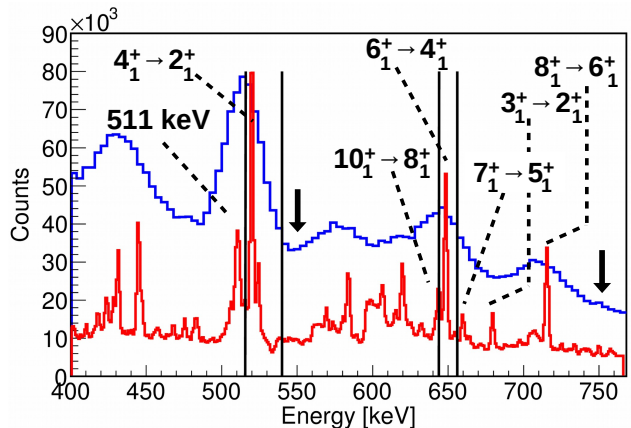


FIG. 6. (Colour online). $E_\gamma(\text{LaBr}_3(\text{Ce}))$ (blue) and $E_\gamma(\text{HPGe})$ (red) spectra obtained in coincidence with the background-subtracted HPGe gates on the $2_1^+ \rightarrow 0_{g.s.}^+$, $8_1^+ \rightarrow 6_1^+$ and $10_1^+ \rightarrow 8_1^+$ transitions. $E_\gamma(\text{LaBr}_3(\text{Ce}))$ gates on the $4_1^+ \rightarrow 2_1^+$ and $6_1^+ \rightarrow 4_1^+$ transitions are indicated by the black solid lines. In order to minimize the contributions of contaminant peaks, observable in the $E_\gamma(\text{HPGe})$ spectrum, these were not centred around the $\text{LaBr}_3(\text{Ce})$ energy peaks. Background gates for the timing information in the $\text{LaBr}_3(\text{Ce})$ array are indicated by the black arrows.

A second indirect measurement was performed on the lifetime of the 4_1^+ level. $E_\gamma(\text{HPGe})$ gates were applied on the $8_1^+ \rightarrow 6_1^+$ and $10_1^+ \rightarrow 8_1^+$ transitions, while $E_\gamma(\text{LaBr}_3(\text{Ce}))$ start and stop gates were applied on the $2_1^+ \rightarrow 0_{g.s.}^+$ and $6_1^+ \rightarrow 4_1^+$ transitions. A background-corrected centroid difference value of $\Delta C = 477(38)$ ps was obtained and by using the time-walk correction $\text{PRD}(648, 333) = 231(6)$ ps, the lifetime $\tau_{2^+} + \tau_{4^+} = 123(19)$ ps was measured. The lifetime of $\tau_{2^+} = 103(10)$ ps was subtracted from this sum of two lifetimes, and the value $\tau_{4^+} = 20(22)$ ps was obtained. The weighted average between the two lifetime measurements (direct and indirect) for the 4_1^+ level gives $\tau_{4^+} = 21(11)$ ps.

C. 6_1^+ level in ^{114}Pd

The lifetime of the 6_1^+ level in ^{114}Pd was determined after gating on the background-subtracted $2_1^+ \rightarrow 0_{g.s.}^+$ and $4_1^+ \rightarrow 2_1^+$ transitions in Gammasphere. $E_\gamma(\text{LaBr}_3(\text{Ce}))$

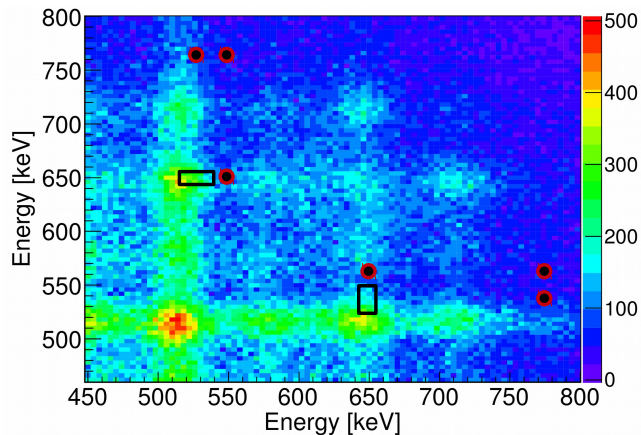


FIG. 7. (Colour online). As Fig. 4 but gated on the background-subtracted $2_1^+ \rightarrow 0_{g.s.}^+$, $8_1^+ \rightarrow 6_1^+$ and $10_1^+ \rightarrow 8_1^+$ transitions, in Gammasphere. The black solid lines define the limits of the gates applied on the delayed and anti-delayed coincidence peaks, while the black dots represent the three background samples selected for each peak.

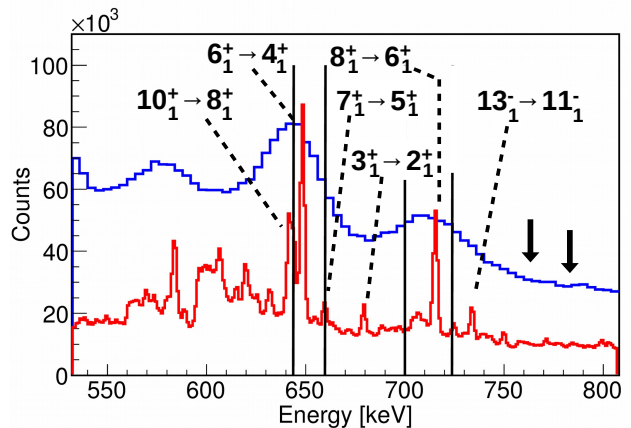


FIG. 8. (Colour online). $E_\gamma(\text{LaBr}_3)$ (blue) and $E_\gamma(\text{HPGe})$ (red) spectra obtained from the two background-subtracted HPGe gates on the $2_1^+ \rightarrow 0_{g.s.}^+$ and $4_1^+ \rightarrow 2_1^+$ transitions. Energy gates on the feeding and depopulating transitions are indicated by the black solid lines. Background gates for the timing information on the LaBr_3 array are indicated by the two black arrows.

(blue) and $E_\gamma(\text{HPGe})$ (red) spectra are shown in Fig. 8. As for the case of the 4_1^+ level, in order to minimize the contribution from the $10_1^+ \rightarrow 8_1^+$ transition, the $E_\gamma(\text{LaBr}_3(\text{Ce}))$ gate on the $6_1^+ \rightarrow 4_1^+$ transition was set asymmetrically to the right-hand side of the peak. Any background gate taken to the immediate right of the 648 keV peak, or to the left of the 715 keV peak, would include also events from the $3_1^+ \rightarrow 2_1^+$ transition, and therefore the background gate for the $6_1^+ \rightarrow 4_1^+$ transition was set around $E_\gamma = 760$ keV. As for the previous case, many peaks can be observed to the left of the $6_1^+ \rightarrow 4_1^+$ transition, and for this reason a left background gate was excluded also for this peak. The background gate for the $8_1^+ \rightarrow 6_1^+$ transition was applied around $E_\gamma = 780$ keV. The positions of the two FEP and the background gates are indicated in Fig. 8 by the two black arrows and by the black dots in the two-dimensional projection of the E_γ - E_γ - ΔT cube, shown in Fig. 9. The measured centroid positions and number of counts for the eight time distributions considered for this measurement, are listed in the bottom part of Table. I. A corrected centroid difference value of $\Delta C^t = 35(15)$ ps was found. Combined with a time-walk correction of $\text{PRD}(715, 648) = 30(4)$ ps the lifetime value obtained was $\tau_{6^+} = 2(8)$ ps. This was translated into an upper limit for this lifetime of 10 ps.

IV. INTERPRETATION OF RESULTS

The Weisskopf hindrance factor F_W is defined as

$$F_W = \frac{\tau_\gamma}{\tau_W}, \quad (7)$$

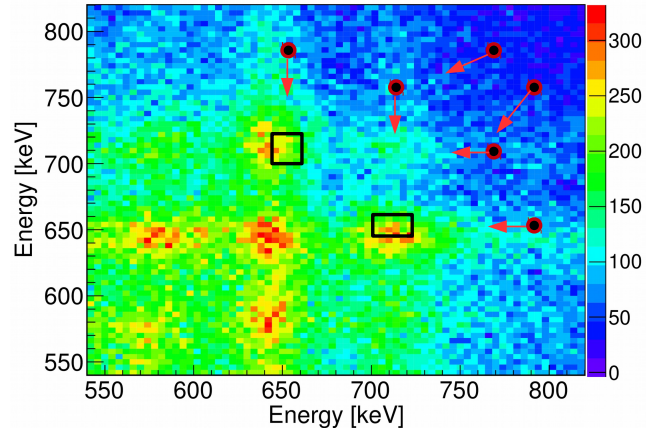


FIG. 9. (Colour online). As for Fig. 4, but obtained by gating on the background-subtracted $2_1^+ \rightarrow 0_{g.s.}^+$, and $4_1^+ \rightarrow 2_1^+$ transitions in Gammasphere. The background regions are indicated by the black dots and the red arrows indicate to which of the two coincidence peaks they refer.

where τ_W is the single-particle Weisskopf estimate of the lifetime and τ_γ is the partial lifetime defined as

$$\tau_\gamma = \tau_{meas}(1 + \alpha), \quad (8)$$

where α is the electron conversion coefficient taken from BrIcc [35]. For each of the three measured lifetimes F_W is in the order of magnitude of 10^{-2} which indicates a collective behaviour for the excited levels in the yrast band of ^{114}Pd .

The $B(E2)$ transition strengths in e^2b^2 units were calculated using the equation

$$B(E2; J_i \rightarrow J_i - 2) = \frac{8.162 \times 10^{10}}{\tau_\gamma E_\gamma^5}, \quad (9)$$

TABLE I. Centroid positions and number of counts for the $p|p$, $p|bg$, $bg|p$ and $bg|bg$ time distributions, obtained for the lifetime measurements of the 2_1^+ , 4_1^+ and 6_1^+ levels in ^{114}Pd . The values are listed for the $p|p$, $p|bg$, $bg|p$ and $bg|bg$ time distributions of both the delayed and anti-delayed coincidence peaks. The centroid positions listed for the background time distributions have been corrected for the Compton time-walk. For each lifetime measurement, the delayed and anti-delayed centroid positions $C^{p|p}$ and the related centroid difference value ΔC are given before and after the background correction from Eq. 3 and labelled with m and t , respectively. The values of the PRD(E_f , E_d) time-walk correction applied in each case are also listed. All centroid positions, PRD values and lifetimes are given in picoseconds.

		2_1^+ level in ^{114}Pd				
Delayed	$C_{p p}^m$	$C_{p bg}^m$	$C_{bg p}^m$	$C_{bg bg}^m$	$C_{p p}^t$	
	130(2)	135(4)	87(4)	98(7)	163(14)	
Anti-del.	$n_{p p}^m$	$n_{p bg}^m$	$n_{bg p}^m$	$n_{bg bg}^m$	$n_{p p}^t$	
	15552(125)	7382(72)	8516(98)	5250(91)	4904(196)	
Delayed	$C_{p p}^m$	$C_{p bg}^m$	$C_{bg p}^m$	$C_{bg bg}^m$	$C_{p p}^t$	
	-148(2)	-141(4)	-117(4)	-132(8)	-195(13)	
Anti-del.	$n_{p p}^m$	$n_{p bg}^m$	$n_{bg p}^m$	$n_{bg bg}^m$	$n_{p p}^t$	
	16024(127)	7080(69)	8811(100)	4963(86)	5096(195)	
		$\Delta C^m = 278(3)$	$\Delta C^t = 358(19)$	PRD = 152(6)	$\tau_{\text{meas}} = \mathbf{103(10)} \rightarrow \text{w.a. } \tau_{2^+} = \mathbf{113(5)}$	
		4_1^+ level in ^{114}Pd				
Delayed	$C_{p p}^m$	$C_{p bg}^m$	$C_{bg p}^m$	$C_{bg bg}^m$	$C_{p p}^t$	
	39(4)	43(5)	32(11)	31(11)	41(21)	
Anti-del.	$n_{p p}^m$	$n_{p bg}^m$	$n_{bg p}^m$	$n_{bg bg}^m$	$n_{p p}^t$	
	2797(53)	899(30)	1390(37)	468(22)	976(75)	
Delayed	$C_{p p}^m$	$C_{p bg}^m$	$C_{bg p}^m$	$C_{bg bg}^m$	$C_{p p}^t$	
	-58(4)	-42(5)	-40(11)	-36(11)	-75(15)	
Anti-del.	$n_{p p}^m$	$n_{p bg}^m$	$n_{bg p}^m$	$n_{bg bg}^m$	$n_{p p}^t$	
	2825(53)	874(30)	1180(34)	581(24)	1352(74)	
		$\Delta C^m = 97(6)$	$\Delta C^t = 116(26)$	PRD = 71(5)	$\tau_{4^+} = 22(13)$	
		$\Delta C^m = 411(11)$	$\Delta C^t = 477(38)$	PRD = 231(6)	$\tau_{4^+} = 20(22) \rightarrow \text{w.a. } \tau_{4^+} = \mathbf{21(11)}$	
		6_1^+ level in ^{114}Pd				
Delayed	$C_{p p}^m$	$C_{p bg}^m$	$C_{bg p}^m$	$C_{bg bg}^m$	$C_{p p}^t$	
	7(3)	5(6)	11(5)	19(8)	11(10)	
Anti-del.	$n_{p p}^m$	$n_{p bg}^m$	$n_{bg p}^m$	$n_{bg bg}^m$	$n_{p p}^t$	
	3664(61)	1543(39)	1145(34)	639(25)	1616(84)	
Delayed	$C_{p p}^m$	$C_{p bg}^m$	$C_{bg p}^m$	$C_{bg bg}^m$	$C_{p p}^t$	
	-27(4)	-22(5)	-35(6)	-20(9)	-24(11)	
Anti-del.	$n_{p p}^m$	$n_{p bg}^m$	$n_{bg p}^m$	$n_{bg bg}^m$	$n_{p p}^t$	
	3512(59)	1522(39)	1011(32)	617(25)	1596(82)	
		$\Delta C^m = 34(5)$	$\Delta C^t = 35(15)$	PRD = 30(4)	$\tau_{\text{meas}} = \mathbf{2(8)} \rightarrow \tau_{6^+} \leq \mathbf{10}$	

where τ_γ is in nanoseconds and the energy E_γ of the transition is in keV. The uncertainties $\sigma_{B(E2)}$ are assumed to be symmetric, and were estimated following the procedure given in Ref. [36]. This is usually recommended when the uncertainties associated to the lifetime measurements are either asymmetric or exceed 10%. Intrinsic quadrupole moments Q_0 for the levels of interest were calculated using the relationship between $B(E2; J \rightarrow J-2)$ and Q_0 , described by the equation

$$B(E2; J_i \rightarrow J_f) = \frac{5}{16\pi} e^2 Q_0^2 \langle J_i K 2 0 | J_f K \rangle^2, \quad (10)$$

where the symbol in brackets $\langle \dots \rangle$ is the Clebsch-Gordon coefficient. Uncertainties on Q_0 were obtained by propagating the uncertainties on $B(E2)$. Deformation parameters $|\beta_2|$ for each level were calculated solving the cubic equation [1]

$$Q_0 = \frac{3}{\sqrt{5}\pi} R_{av}^2 Z \beta_2 \left(1 + \frac{2}{7} \sqrt{\frac{5}{\pi}} \beta_2 + \frac{1}{14\pi} \beta_2^2 + \dots \right), \quad (11)$$

valid in the assumption of a quadrupoloid shape. The value of $R_{av} = 1.2 \cdot A^{1/3}$ fm was used. Uncertainties for the different $|\beta_2|$ values were obtained solving the same equation for the upper and lower limits of Q_0 . Partial

level lifetimes τ_γ , reduced transition probabilities $B(E2)$,⁴⁸⁴
intrinsic quadrupole moments Q_0 and deformation pa-⁴⁸⁵
rameters $|\beta_2|$ for the 2_1^+ , 4_1^+ and 6_1^+ levels in ^{114}Pd are
listed in Table. II.

TABLE II. Partial lifetimes τ_γ , reduced transition probabili-
ties $B(E2; J_i \rightarrow J_i - 2)$ together with intrinsic quadrupole
moments Q_0 and deformation parameters $|\beta_2|$ for ^{114}Pd . One
W.u. equals $32.84 \times 10^{-4} e^2 b^2$.

J_i^π	τ_γ [ps]	$B(E2; J_i \rightarrow J_i - 2)$ [$e^2 b^2$]	Q_0 [W.u.]	$ \beta_2 $ [eb]
2_1^+	115(5)	0.174(7)	53(2)	2.96(6)
4_1^+	21(11)	0.140(73)	43(27)	2.22(58)
6_1^+	≤ 10	≥ 0.071	≥ 21	≥ 1.51

In Davydov-Filippov's model [17] for rigid triaxial ro-⁴⁸⁶
tators, $B(E2)$ values between the ground-state band and⁴⁸⁷
quasi- γ band are able to provide a signature of triaxial-⁴⁸⁸
ity, however, as shown in Ref. [37], for values of γ go-⁴⁸⁹
ing from 0° to 60° , $B(E2)$ values for transitions between⁴⁹⁰
levels inside the ground-state band change by less than⁴⁹¹
10%, which is below the experimental uncertainties on⁴⁹²
the $B(E2)$ values presented in this work.

Figure 10 shows the comparison between measured⁴⁹³
 $B(E2)$ values (black dots) and theoretical values from,⁴⁹⁴
Projected Shell Model (PSM) [14] (squares) and using⁴⁹⁵
the Bohr Hamiltonian coupled with the Killingbeck po-⁴⁹⁶
tential [20] (triangles, down). In this last work ^{114}Pd ⁴⁹⁷
was assumed to be triaxial. In the IBM-1 calculations in⁴⁹⁸
Ref. [38] two different approaches were used to calculate⁴⁹⁹
 $B(E2)$ transition rates in ^{114}Pd . An $\text{SU}(3)$ -type Hamil-⁵⁰⁰
tonian was used first (triangles, up), and then a three-⁵⁰¹
body term (three d bosons) able to create a triaxial min-⁵⁰²
imum in the potential was added (crosses). The effect of⁵⁰³
this additional interaction is to strongly modify the dis-⁵⁰⁴
tribution of the energy levels belonging to the γ -band,⁵⁰⁵
reducing the odd-even staggering $S(J)$ described previ-⁵⁰⁶
ously [39]. As pointed out in Ref. [38], the three-body⁵⁰⁷
term reduces the relative $B(E2)$ values for the ground-⁵⁰⁸
state band, by a factor of ~ 0.8 , leading to a better agree-⁵⁰⁹
ment with the experimental $B(E2)$ values as shown in⁵¹⁰
Figure 10. IBM-2 calculations [40] (not in the figure) gives⁵¹¹
a relative $B(E2; 4_1^+ \rightarrow 2_1^+)$ value of $0.25 e^2 b^2$ which over-⁵¹²
laps with those from PSM and the triaxial IBM-1 (the⁵¹³
 $B(E2; 6_1^+ \rightarrow 4_1^+)$ value was not calculated in this model).⁵¹⁴
All calculations were normalized to the $B(E2; 2_1^+ \rightarrow 0_1^+)$ ⁵¹⁵
value measured in this work.

Figure 10 shows that none of the calculations for the⁵¹⁷
 $B(E2; 4_1^+ \rightarrow 2_1^+)$ value are within one standard devia-⁵¹⁸
tion of the experimental value but the closest is for the⁵¹⁹
Killingbeck potential which is at 1.2 standard deviations.⁵²⁰
This calculation explicitly includes the triaxial deforma-⁵²¹
tion and this may be why it shows better agreement. In-⁵²²
deed, the $B(E2; 4_1^+ \rightarrow 2_1^+)$ values calculated in the two⁵²³
versions of the IBM-1 show the importance of triaxiality.⁵²⁴
However, in order to get a better understanding, it would⁵²⁵
be necessary to measure the lifetimes of the first excited⁵²⁶

states of the quasi- γ band, which is not possible with this
data set.

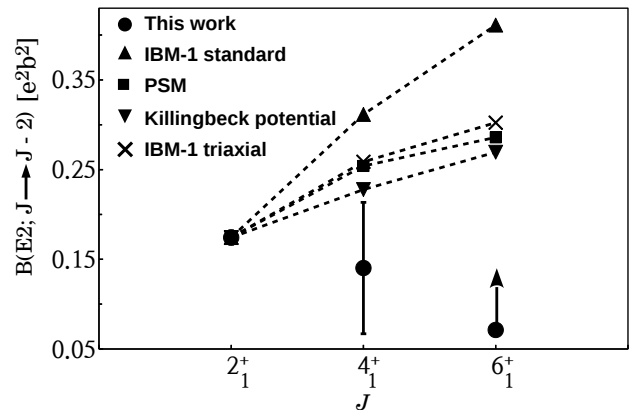
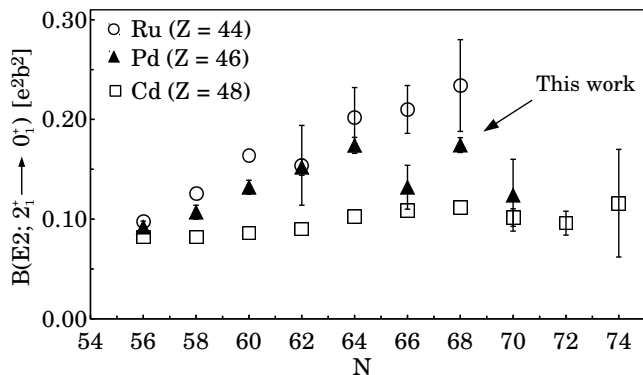


FIG. 10. Theoretical values of the reduced transition probabili-
ties for the $2_1^+ \rightarrow 0_{g.s.}^+$, $4_1^+ \rightarrow 2_1^+$ and $6_1^+ \rightarrow 4_1^+$ transi-
tions in ^{114}Pd , obtained from PSM (squares) [14], Killingbeck po-
tential (triangles, down) [20], standard IBM-1 (triangles, up),
and triaxial IBM-1 (crosses) [38], compared with experimen-
tal values (black dots).

Additional information can be obtained by analysing
the systematics of the $B(E2; 2_1^+ \rightarrow 0_1^+)$ values for the
neighbouring even- Z isotopic chains, i.e. Cd and Ru as
shown in Fig. 11. Even-even cadmium isotopes in the
range $N = 56-72$ are considered to be good examples of
spherical anharmonic vibrators [9, 41, 42] while among
the even-even Ru isotopes cases of γ -softness and stable
triaxiality in the range $^{100-118}\text{Ru}$ were observed [6, 7].
Fig. 11 shows that as the number of neutrons N increases,
the Ru and Cd isotopic chains follow completely differ-
ent paths. The $B(E2)$ values for the cadmium chain are
rather constant while Ru transition rates increases up
to a maximum value for ^{112}Ru , where the maximum of
triaxiality is expected to occur [6]. The $B(E2)$ values
for the Pd chain lie in between those of Cd and Ru for
almost every value of N , but it is interesting that the
adopted value of ^{114}Pd approaches that of ^{112}Ru , indi-
cating some degree of triaxiality. Moreover, Q_0 values in
the ground-state band of molybdenum and ruthenium,
which are associated to γ -deformation, were observed to
decrease for increasing J values [4] and this is consistent
with the values quoted in Table II for the 2^+ and 4^+ lev-
els in ^{114}Pd .

Figure 11 also hints at some sort of staggering behaviour
between ^{112}Pd and ^{116}Pd . However, the lifetime mea-
surements of the first 2^+ levels in ^{112}Pd and ^{116}Pd
have been performed using the recoil distance method
in Refs. [43] and [44], respectively. In both works, the
palladium isotopes were observed following the sponta-
neous fission of ^{252}Cf and γ rays were detected in singles,
in coincidence with fission fragments. Considering that
lifetimes were obtained by measuring the absolute or rela-
tive intensities of the $2_1^+ \rightarrow 0_1^+$ transition in the two
nuclei and that high- J levels are likely to be populated,

527 it is possible that some feeding transitions contribute to
 528 the lifetimes measured in the two experiments. The life-
 529 time measured would then be larger than that for the 2_1^+
 530 level leading to correspondingly smaller $B(E2; 2_1^+ \rightarrow 0_1^+)$
 531 values.



532

533 FIG. 11. $B(E2; 2_1^+ \rightarrow 0_1^+)$ transition rates for the Ru
 534 ($Z = 44$, circles), Pd ($Z = 46$, triangles) and Cd ($Z = 48$,
 535 squares) isotopic chains. Values are taken from Ref. [36], ex-
 536 cept for ^{114}Pd ($N = 68$) which corresponds to $\tau_{2^+} = 113(5)$ ps.
 537 Error bars are not shown when they are smaller than the data
 538 points.

539

540
 541 The ratio $R_{B(E2)} = B(E2; 4_1^+ \rightarrow 2_1^+) / B(E2; 2_1^+ \rightarrow 0_1^+)$
 542 is indicative of the degree of collectivity: $R_{B(E2)} = 2$ for
 543 vibrational nuclei [25], 1.43 for rigid axial nuclei [45], 1.68
 544 for γ -unstable rotors [46] and 1.40 for rigid triaxial ro-
 545 tors [47], in the case of $\gamma = 27.5^\circ$. The $B(E2; J_i \rightarrow J_i - 2)$
 546 values in Table II give a value of $R_{B(E2)} = 0.80(42)$
 547 for ^{114}Pd and this is compared with the experimental
 548 ratios measured in Coulomb excitation experiments for
 549 $^{104,106,108,110}\text{Pd}$ in Fig. 12. It can be observed that the
 550 $R_{B(E2)}$ values of Pd isotopes for $N = 60, 62, 64$ fluctu-
 551 ate around the limit of 1.68 given by the Wilets-Jean's
 552 model, although the value for ^{104}Pd ($N = 58$) is slightly
 553 smaller. A sudden drop of the $R_{B(E2)}$ value is observed
 554 for $N = 68$ and while the experimental value is more than
 555 1 standard deviation from the value for either rigid axial
 556 or triaxial deformation, it is consistent within 1.4σ with
 557 the conclusion suggested by the energy staggering $S(J)$,
 558 shown in Fig. 1, that there is an inversion to rigid triaxial
 559 behaviour at ^{114}Pd .

560

V. CONCLUSIONS

561 This work reports on the first measurements of life-
 562 times of excited levels in fission fragments using the large
 563 scale array Gammasphere + FATIMA. The hybrid array,
 564 used at the Argonne National Laboratory used 51 HPGe
 565 detectors coupled to 25 $\text{LaBr}_3(\text{Ce})$ scintillators. A fully-
 566 digital acquisition set-up was used for the first time.
 567 A lifetime measurement of the 2_1^+ level in ^{114}Pd gave a
 568 value of $\tau_{2^+} = 103(10)$ ps which was found to be con-
 569 sistent with previous measurements [15, 34]. Values of

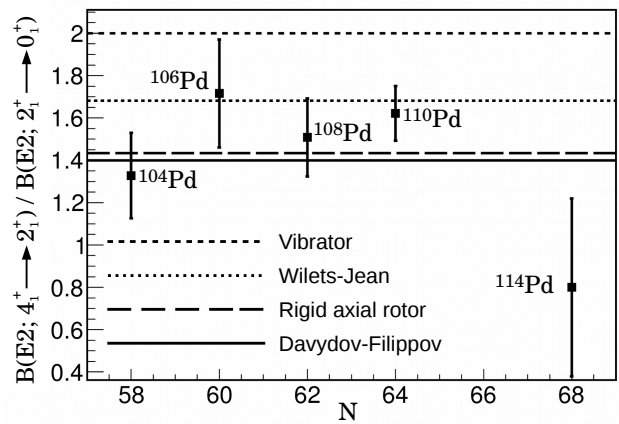


FIG. 12. Experimental $R_{B(E2)}$ values for $^{104,106,108,110}\text{Pd}$,
 taken from Ref. [27], and for ^{114}Pd measured in this work.
 The ratios are compared with the values predicted by
 the vibrator, rigid axial rotor, Wilets-Jean's and Davy-
 dov-Filippov's models, as indicated in the legend.

$\tau_{4^+} = 22(13)$ ps and $\tau_{6^+} \leq 10$ ps were also obtained.
 From the lifetimes measured, $B(E2)$ transition strengths
 and quadrupole moments Q_0 were calculated, along with
 their associated deformation parameters $|\beta_2|$. None of
 the theoretical calculations performed using the IBM[38–
 40], PSM [14], and Collective model calculations [20] is
 within 1σ of the measured $B(E2; 4_1^+ \rightarrow 2_1^+)$ value but the
 closest is the one obtained from the Killingbeck potential,
 probably because of the inclusion of a triaxial minimum.
 The lower limit obtained for the $B(E2; 6_1^+ \rightarrow 4_1^+)$ value
 is in agreement with all the calculations.

The suggestion that ^{114}Pd is one of the most de-
 formed of all Pd isotopes is strongly supported by the
 $B(E2; 2_1^+ \rightarrow 0_1^+)$ value which is one of the largest of
 the isotopic chain. The systematics of the $B(E2)$ values
 for even-even palladium isotopes compared with the ones
 of the even-even neighbouring ruthenium and cadmium
 isotopes shows an onset of triaxiality that reaches a max-
 imum for ^{114}Pd .

The experimental $R_{B(E2)}$ ratio was compared with the
 expectations from different models and a transition from
 γ -soft rotor to that of a rigid triaxially-deformed con-
 figuration seems to be taking place for $N = 68$.

Any measurement of inter-band $B(E2)$ values was pre-
 cluded by the lack of statistics, with $\text{LaBr}_3(\text{Ce})$ detectors,
 for the transitions between the quasi- γ and ground-state
 bands. This forbids any quantitative evaluation of the
 triaxial deformation characterising ^{114}Pd and therefore
 new data will be necessary to draw any definitive conclu-
 sion.

ACKNOWLEDGMENTS

This work was financially supported by the Sci-
 ence and Technology Facility Council (STFC) grants

ST/L005840/1, ST/L005743/1 and ST/G000751/1. This work has also been partially supported by the U.S. Department of Energy, Office of Science, Office of Nuclear Physics under contract DE-AC02-06CH11357 (ANL). The author E. R. Gamba would like to acknowledge the STFC for founding his Ph.D. studentship. D. J. Hartley acknowledges the National Science Foundation, Grant No. PHY-1502092. E. A. Stefanova and O. Yordanov would like to acknowledge the project DFNI-E02/6. This research used resources of the Argonne National Laboratory ATLAS facility, which is a DOE Office of Science User Facility.

-
- [1] K. E. G. Lobner, M. Vetter and V. Höning, Nucl. Data Tables 7 (1970) 495.
- [2] A. Bohr, K. Dan. Vidensk. Selsk. Mat-Fys. 26 (1952) 14.
- [3] H. Watanabe *et al.*, Phys. Lett. B 704 (2011) 270.
- [4] J. B. Snyder *et al.*, Phys. Lett. B 723 (2013) 61.
- [5] Y. X. Luo *et al.*, Phys. Lett. B 670 (2009) 307.
- [6] D. T. Doherty *et al.*, Phys. Lett. B 76 (2017) 334.
- [7] P.-A. Söderström *et al.*, Phys. Rev. C 88 (2013) 024301.
- [8] S. Lalkovski *et al.*, Eur. Phys. J. A 18 (2003) 589.
- [9] Y. X. Luo *et al.*, Nucl. Phys. A 874 (2012) 32.
- [10] L. E. Svensson *et al.*, Nucl. Phys. A 584 (1995) 547.
- [11] Y. Wang *et al.*, Phys. Rev. C 63 (2001) 024309.
- [12] X. Q. Zhang, J. H. Hamilton, A. V. Ramayya, S. J. Zhu, J. K. Hwang, C. J. Beyer, J. Kormicki, E. F. Jones, P. M. Gore *et al.*, Phys. Rev. C 63 (2001) 027302.
- [13] M. A. Stoyer *et al.*, Nucl. Phys. A 787 (2007) 455c.
- [14] R. Chaudhary *et al.*, Eur. Phys. J Plus 133 (2018) 81.
- [15] A. Dewald, K. Starosta, P. Petkov, M. Hackstein, W. Rother, P. Adrich, A. M. Amthor, T. Baumann, D. Bazin *et al.*, Phys. Rev. C 78 (2008) 051302(R).
- [16] L. Wilets and M. Jean, Phys. Rev. 102 (1956) 788.
- [17] A. S. Davydov and G. F. Filippov, Soviet Physics JETP 6 (1958) 33.
- [18] N. V. Zamfir and R. F. Casten, Phys. Lett. B 260 (1991) 265.
- [19] S. Frauendorf, Int. Jour. Mod. Phys. 24 (2015) 1541001.
- [20] H. Sobhani *et al.*, Nucl. Phys. A 973 (2018) 33.
- [21] A. C. Wahl, Symposium on Physics and Chemistry of Fission, IAEA, Vienna, 1965.
- [22] A. Arima and F. Iachello, Phys. Rev. Lett. 35 (1975) 1069.
- [23] F. Iachello and A. Arima, The Interacting Boson Model (Cambridge University Press, 1987).
- [24] K. Hara and Y. Sun, Int. Journ. of Mod. Phys. (1995), 637.
- [25] A. Bohr and B. R. Mottelson, Nuclear Structure - Volume 1 and 2 (World Scientific, Singapore, 1975).
- [26] J. Killingbeck, J. Phys. A: Math. Gen. 13 (1980), L393.
- [27] <https://www.nndc.bnl.gov>.
- [28] I-Y.Lee *et al.*, Nuclear Physics A 520 (1990) 641c .
- [29] O. J. Roberts *et al.*, Nucl. Instrum. Methods Phys. Res. Sect. A 748 (2014) 91.
- [30] L. M. Fraile *et al.*, FATIMA technical design report, 2105.
- [31] M. Rudigier *et al.*, Acta Physica Polonica B 48 (2017) 351.
- [32] J.-M Régis *et al.*, Nucl. Instrum. Methods Phys. Res. Sect. A 726 (2013) 191.
- [33] E. R. Gamba, A. M. Bruce and M. Rudigier, Nucl. Instrum. Methods Phys. Res. Sect. A 928 (2019) 93.
- [34] H. Mach *et al.*, JYFL annual report, 2003.
- [35] <http://bricc.anu.edu.au>.
- [36] S. Raman, C. J. Nestor, and P. Tikkanen, At. Data Nucl. Data Tables 78 (2001) 1.
- [37] H. Toki and A. Faessler, Z. Phys. A 276 (1976) 35.
- [38] B. Sorgunlu and P. Van Isacker, Nucl. Phys. A 808 (2008) 27.
- [39] P. Van Isacker, private communication.
- [40] K.-H. Kim *et al.*, Nucl. Phys. A 604 (1996) 163.
- [41] A. Jokinen *et al.*, Proceedings of the third international conference on “Fission and properties of neutron-rich nuclei”, USA, 2002.
- [42] A. Arahamian *et al.*, Phys. Lett. B 140 (1984) 22.
- [43] G. Mamane *et al.*, Nucl. Phys. A 454 (1986) 213.
- [44] R. C. Jared, presented at the third symposium on the physics and chemistry of fission, Rochester, New York, 1973.
- [45] G. Alaga, K. Aider, A. Bohr and B. Mottelson, Mat. Fys. Medd. Dan. Vid. Selsk. 29 (1955).
- [46] F. Iachello, Phys. Rev. Lett. 85 (2000) 3580.
- [47] A. S. Davydov and V. S. Rostovski, Nucl. Phys. 12 (1959), 58.